small
NANO MICRO
www.small-journal.com

Imparting Designer Biorecognition Functionality to Metal–Organic Frameworks by a DNA-Mediated Surface Engineering Strategy

Weiyu Ning, Zhenghan Di, Yingjie Yu, Pingmei Zeng, Chunzhi Di, Daquan Chen, Xueqian Kong, Guangjun Nie, Yuliang Zhao, and Lele Li**

Surface functionality is an essential component for processing and application of metal–organic frameworks (MOFs). A simple and cost-effective strategy for DNA-mediated surface engineering of zirconium-based nanoscale MOFs (NMOFs) is presented, capable of endowing them with specific molecular recognition properties and thus expanding their potential for applications in nanotechnology and biotechnology. It is shown that efficient immobilization of functional DNA on NMOFs can be achieved via surface coordination chemistry. With this strategy, it is demonstrated that such porphyrin-based NMOFs can be modified with a DNA aptamer for targeting specific cancer cells. Furthermore, the DNA–NMOFs can facilitate the delivery of therapeutic DNA (e.g., CpG) into cells for efficient recognition of endosomal Toll-like receptor 9 and subsequent enhanced immunostimulatory activity in vitro and in vivo. No apparent toxicity is observed with systemic delivery of the DNA–NMOFs in vivo. Overall, these results suggest that the strategy allows for surface functionalization of MOFs with different functional DNAs, extending the use of these materials to diverse applications in biosensor, bioimaging, and nanomedicine.

1. Introduction

Metal–organic frameworks (MOFs), constructed by self-assembly of metal ions/clusters and organic ligands through coordination interactions, have been gaining momentum from both the fundamental and technological perspectives due to their chemical versatility with functionality suitable to various applications.[1–12] In particular, there has been growing interest in "Zr_6 MOFs," which are built from the well-known $Zr_6O_4(OH)_4$ octahedral secondary building units.[13,14] These Zr_6 MOFs exhibit high thermal and chemical stability due to strong coordination bonds between the Zr_6 nodes and the organic linkers, and are therefore offering wider opportunities for a variety of uses, including gas storage, catalysis, and drug delivery.[12–17] Despite exhaustive efforts, a formidable challenge in this field is the lack of general approaches for the synthesis of biocompatible MOFs with specific molecular recognition capabilities, which is a prerequisite for their commonly proposed biomedical applications. To overcome this limitation, much effort has been devoted to develop new modification technologies for the surface engineering of MOFs with biological ligands for specific molecular recognition.[18–20] However, the reported conjugation methods are mainly based on incorporating pendant reactive moieties (e.g., $-NH_2$, $-N_3$, $-COOH$) on the organic linkers to provide postmodification sites, which were often expensive, time-consuming, and lack efficiency, in many cases precluding direct synthesis and affecting the underlying crystalline structure.

Recently, Farha and co-workers reported a simple and facile postsynthetic modification strategy termed solvent-assisted ligand-incorporation to decorate the metal nodes of MOFs with carboxylate- or phosphonate-terminated small molecules.[21–30] Since the pioneering work on functionalization of nanoscale MOFs (NMOFs) with nucleic acids through metal–phosphate coordination interaction was reported by Lin and co-workers,[31] it has witnessed an explosion of interest in the development of DNA-attached NMOFs for a variety of applications such as

W. Ning, Z. Di, C. Di, Prof. G. Nie, Prof. Y. Zhao, Prof. L. Li
CAS Key Laboratory for Biomedical Effects of Nanomaterials and Nanosafety
CAS Center for Excellence in Nanoscience, National Center for Nanoscience and Technology (NCNST)
Beijing 100190, China
E-mail: zhaoyl@nanoctr.cn; lilele@nanoctr.cn
Dr. Y. Yu
Department of Materials Science and Engineering
Stony Brook University
Stony Brook, NY 11794, USA
P. Zeng, Prof. X. Kong
Center for Chemistry of High-Performance & Novel Materials
Department of Chemistry
Zhejiang University
Hangzhou 310027, China
Prof. D. Chen
School of Pharmacy
Yantai University
Yantai 264005, China
The ORCID identification number(s) for the author(s) of this article can be found under https://doi.org/10.1002/smll.201703812.
DOI: 10.1002/smll.201703812

programmable nanoparticle (NP) assembly,[32,33] gene and immunostimulatory oligonucleotide delivery.[31,34] Herein, we developed a simple strategy for functional DNA-mediated surface engineering of porphyrin-based Zr_6 NMOFs capable of imparting biorecognition functionalities to their surface. DNA–NMOFs with designer recognition property were constructed through this approach for targeted cancer imaging and specific immune activation.

2. Results and Discussion

PCN-224, a porphyrinic Zr_6 MOF, was chosen as a model system for demonstrating the benefits of the approach due to its exceptional stability, good biocompatibility, and good optical properties.[14] Nanoscale PCN-224 MOFs were synthesized through a reported bottom-up approach.[15] Then, we prepared DNA-functionalized NMOFs by using a random DNA (30-mer poly A) through coordination interaction of its phosphate groups with coordinatively unsaturated metal sites of Zr_6 cluster on the surface of MOF NPs (**Figure 1**). The DNA attachment was directly confirmed by the quantification of Cy3 dye-labeled DNA molecules on the purified NMOFs, which was estimated to be 9.7 nmol DNA per mg nanoparticles. Representative transmission electron microscopy (TEM) images of the NMOFs show that they display uniform spherical morphology with mean sizes of ≈90 nm (**Figure 2**A). The resulting DNA–NMOFs remained monodisperse in size without obvious shape change and aggregation (Figure 2B). Long-term investigation by TEM revealed that DNA–NMOFs are stable in H_2O even after 7 d (Figure S1, Supporting Information). Dynamic light scattering (DLS) measurements indicated that the hydrodynamic size of the NMOFs changed from 126. to 144.7 nm after DNA attachment (Figure 2C), this 18.3 nm increase in diameter is consistent with the addition of a single-stranded DNA shell onto the NMOFs. Zeta potential measurement showed that NMOFs were positively charged (16.1 mV) and became highly negatively charged (–27.8 mV) after the surface functionalization with DNA (Figure 2D), suggesting successful DNA attachment on the NMOF surface. ^{31}P solid-state nuclear magnetic resonance (SSNMR) was employed to probe chemical interaction between the DNA and the NMOFs in the DNA–MOF nanoparticles (Figure S2, Supporting Information). The Zr–phosphate

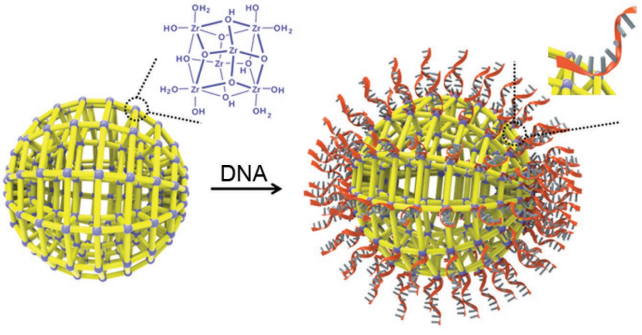

Figure 1. Schematic illustration of DNA functionalization of NMOFs through multivalent coordination interactions between the Zr_6 clusters and the DNA phosphate backbone.

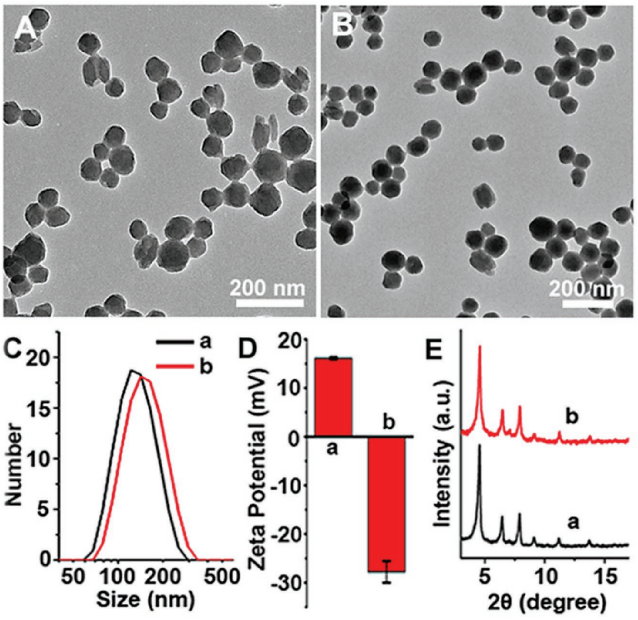

Figure 2. TEM images of the A) as-synthesized NMOFs and B) DNA-functionalized NMOFs. C) DLS, D) zeta potential, and E) PXRD of the (a) NMOFs and (b) DNA-functionalized NMOFs.

bond formation in the DNA–MOFs is directly observed as the upfield shift from –2.6 ppm (corresponding to ^{31}P of unbound phosphodiester) to –6.0 ppm for ^{31}P signal of DNA. The partial shift of the phosphorus resonances indicates that only part of the DNA is attached to the NMOF surface. Powder X-ray diffraction (PXRD) data confirmed that PCN-224 NMOFs functionalized with DNA molecules still retained their crystallinity (Figure 2E). The corresponding absorption and emission spectra of DNA–NMOFs are similar to that of the as-prepared NMOFs

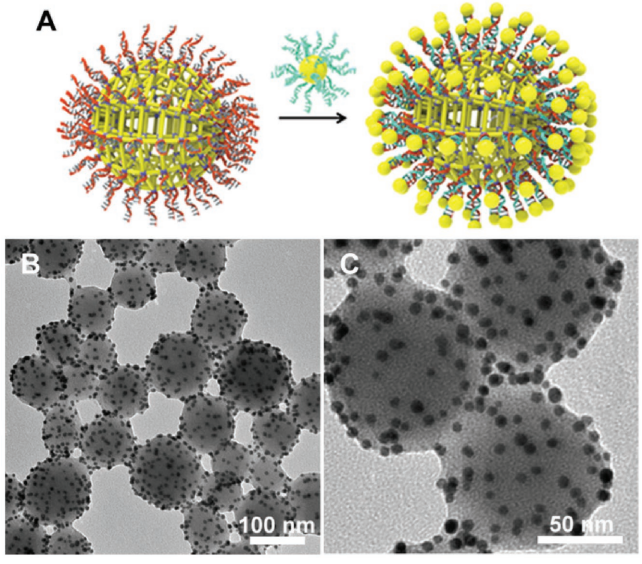

Figure 3. A) Schematic illustration showing the DNA-mediated assembly of NMOFs with AuNPs. B,C) TEM images of A30–NMOFs assembled with complementary DNA-modified AuNPs.

(Figure S3, Supporting Information), implying that the characteristic optical property of the NMOFs was also maintained.

DNA functionalization can endow the nanoparticles with addressability of DNA. To probe the functionality of the DNA on the DNA–NMOFs, we allowed the NMOFs functionalized with A30 oligonucleotides (ODNs) (A30–NMOFs) to assemble with T30-modified 5 nm AuNPs (T30–AuNPs) (**Figure 3**A). As shown in Figure 3B,C, the A30–NMOFs were surrounded by a number of T30–AuNPs, forming satellite assemblies. As expected, control experiments using AuNPs modified with a noncomplementary DNA strand (A30–AuNPs) did not yield efficient NP assembly (Figure S4, Supporting Information). These results confirmed that the DNA was not only attached to NMOFs in large numbers but also retained their ability to hybridize to complementary DNA targets. Therefore, it should be possible to further functionalize the NMOFs with specific DNA based on the complementary base-pairing interactions, thus is of great importance for their future biomedical applications. Moreover, since this approach relies only on the surface properties of the MOFs, it is generally applicable to many other

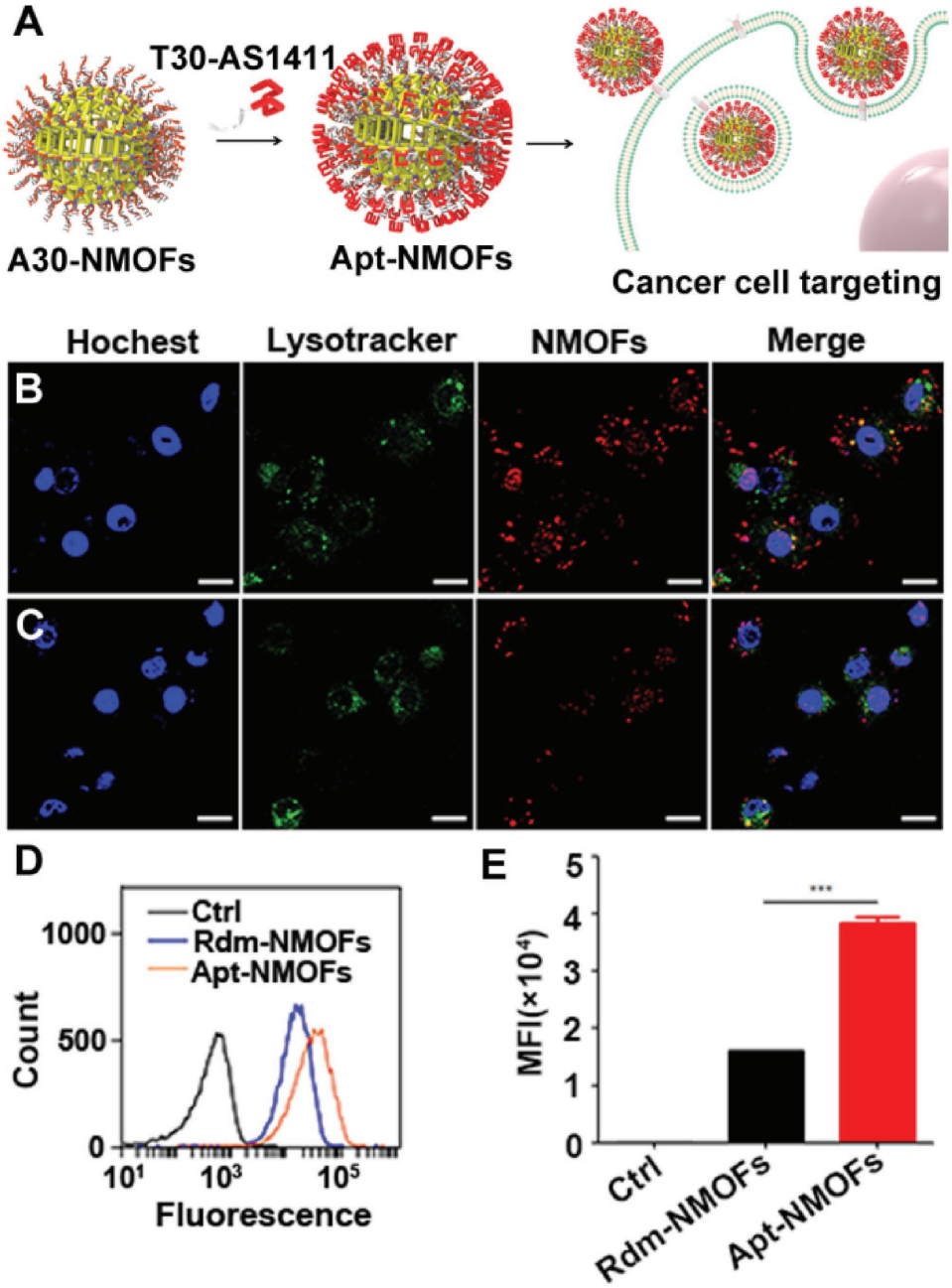

Figure 4. A) Schematic illustration showing functionalization of NMOFs with DNA aptamer for targeting specific cancer cells. Confocal microscopy images of MDA-MB-231 cells treated with B) Apt–NMOFs and C) Rdm–NMOFs. Scale bars = 20 µm. D,E) Flow cytometric quantification of the cellular uptake of Apt–NMOFs and Rdm–NMOFs. Data are represented as means ± standard deviation (SD), $n = 4$, asterisks indicate $P < 0.001$.

Zr_6 MOFs with a variety of compositions, sizes, and shapes. As an example, UiO-66, the first reported Zr_6 MOF,[13] was also modified with DNA though coordination bonds (Figure S5, Supporting Information), highlighting the eligibility of such surface engineering approach. For this strategy, although conjugation of specific DNA on MOFs can be achieved without chemical modification of DNA or MOFs, it requires the preattachment of poly-A for hybridization.

Having established a simple strategy for DNA functionalization of MOFs, we explored use of the approach to endow NMOFs with specific biorecognition capabilities for cancer targeting by introducing DNA aptamers (**Figure 4**A). Aptamers are in vitro selected single-stranded nucleic acids that are able to fold into well-defined conformations to recognize and bind to a wide array of biological targets with high affinity and specificity.[35] As a proof-of-concept experiment, an antinucleolin DNA aptamer AS1411[36] contains 24 extra T bases at the 5′-terminus (5′-T24-GGT GGT GGT GGT TGT GGT GGT GGT GG-3′) was conjugated to A30–NMOF through hybridization (denoted as Apt–NMOFs) for specific targeting of human breast cancer cells MDA-MB-231, because nucleolin was overexpressed on the cell membrane and served as receptor for Apt–NMOFs.[36] As shown in Figure 4B,C, fluorescence microscopy revealed that cells treated with the Apt–NMOFs exhibited more red fluorescence signal of PCN-224 than those incubated with the Rdm–NMOFs that were modified with control DNA with a randomized sequence (Rdm–NMOFs). Additionally, flow cytometry analysis (Figure 4D,E) showed that the fluorescence intensity of MDA-MB-231 cells incubated with Apt–NMOFs was 2.4-fold higher than that of cells treated with Rdm–NMOFs. Since DNAs with high G/C content are known to show high cellular uptake due to the formation of secondary structures,[37] we further used a control DNA sequence with similar G/C content to the aptamer for targeting experiments. The imaging analysis showed that the obtained MOF conjugates resulted in much lower fluorescence in the cells than that in cells treated

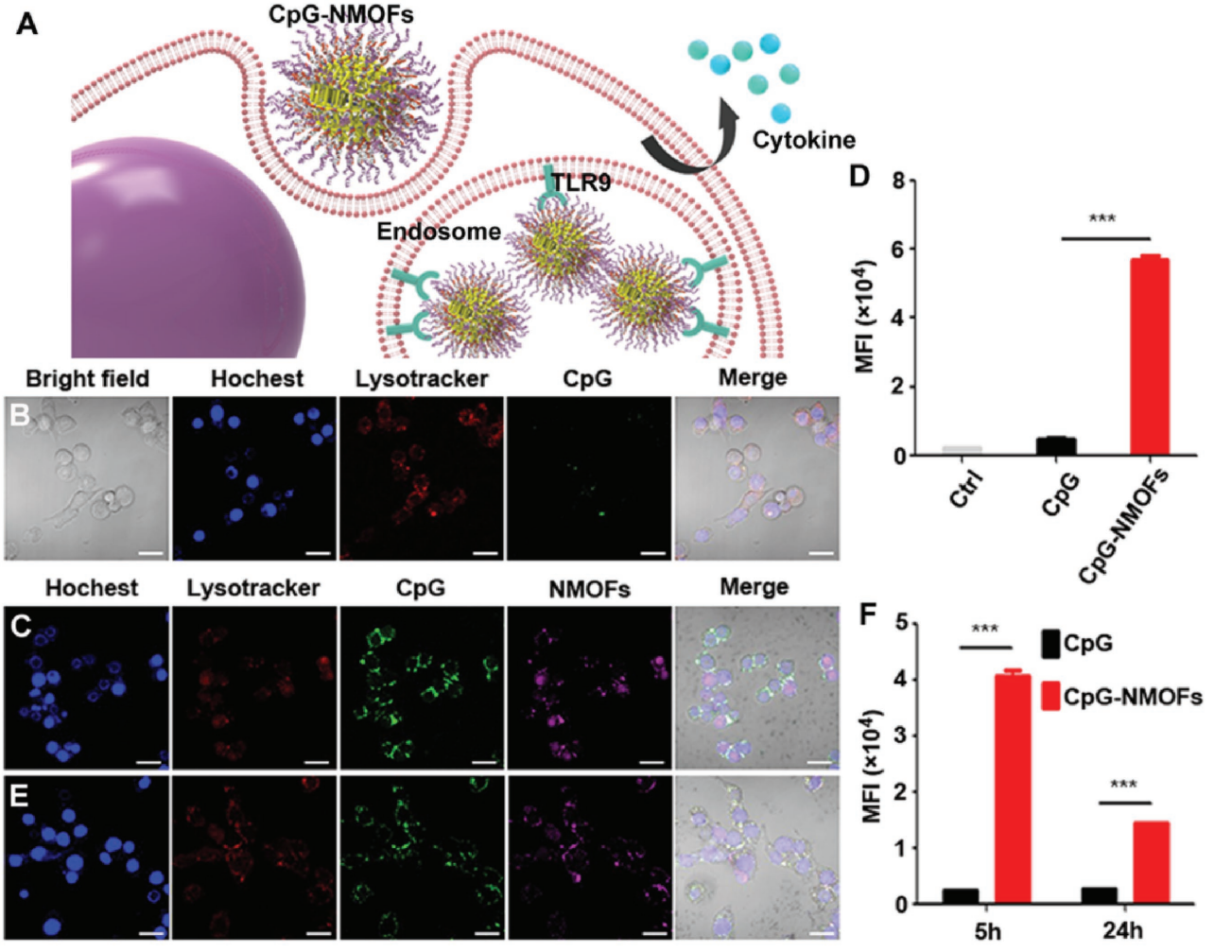

Figure 5. A) Schematic illustration of immunostimulatory effect of the CpG–NMOFs. After entering macrophage cells, the CpG–NMOFs can be recognized by TLR9 in endosome and elicit a immunostimulatory activity. Confocal microscopy images of RAW264.7 macrophage cells incubated with B) free CpG and C) CpG–NMOFs for 2 h. Scale bars = 20 µm. D) Flow cytometric quantification of the cellular uptake of CpG and CpG–NMOFs after 2 h incubation. Data are represented as means ± SD, $n = 4$, asterisks indicate $P < 0.001$. E) Confocal microscopy images of the macrophage cells at 24 h after the initial 2 h incubation with CpG–NMOFs. Scale bars = 20 um. F) Flow cytometric analysis of FAM fluorescence in the cells at 5 and 24 h after the initial 2 h incubation with CpG–NMOFs. Data are represented as means ± SD, $n = 4$, asterisks indicate $P < 0.001$.

with Apt–NMOFs (Figure S6, Supporting Information). Taken together, it could be interpreted that the attachment of AS1411 onto the surface of NMOFs could enhance their cellular uptake efficiency through aptamer-mediated cellular internalization via specific receptor-mediated endocytosis. Given the availability of various aptamers specific for different biotargets, the functionalization of DNA aptamer on MOFs reported herein will advance the application of MOFs in biosensing, diagnosis, and therapy.

We then evaluated the application of these DNA–NMOFs as nanocarriers for therapeutic DNA (e.g., CpG) delivery (**Figure 5**A). CpG ODNs are short single-stranded DNA molecules containing unmethylated cytosine–guanine motifs that are known to recognize and activate Toll-like receptor 9 (TLR9) and have been extensively exploited as immune modulators for many applications including vaccine adjuvants and immunotherapeutic agents.[38,39] CpG ODNs with a T30 tail was successfully conjugated to the A30–NMOFs through DNA hybridization. The loading content of DNA strands on the NMOF is 6.1 nmol mg^{-1} particle. RAW264.7 macrophage cells were incubated with FAM (fluorescein)-labeled CpG ODNs or the NMOFs functionalized with FAM-labeled CpG (CpG–NMOFs) for 2 h in the absence of cationic transfection agents. Confocal microscopy revealed no obvious florescence in the cells incubated with CpG ODNs (Figure 5B), which could be attributed to the low cell membrane permeability of free DNA. In contrast, a high level of FAM fluorescence was observed in the cells treated with CpG–NMOFs (Figure 5C), indicating enhanced internalization of the nanoparticles. The colocalization study showed that CpG–NMOFs were mainly transported to endo-/lysosomal vesicles, which is important for CpG delivery because TLR9 in endo-/lysosomal compartments is the key site of interaction with CpG ODNs for immune stimulation. Flow cytometry was carried out to quantify the fluorescence (Figure 5D), and revealed that the cells incubated with CpG–NMOFs displayed ≈12.0-fold higher FAM fluorescence when compared with the cells treated with free CpG ODNs. These results show that, despite their highly negative charge, DNA–NMOFs are readily internalized by cells without the need for transfection agents, which is consistent with the reported cellular uptake characteristics of spherical nucleic acid nanoparticle conjugates.[40,41]

Since it is highly desirable for CpG ODNs to be retained in the cells as long as possible to continuous stimulate endosomal TLR9 and thus enhance the immunostimulatory activity, we next sought to investigate the clearance of CpG–NMOFs in cells after 2 h treatment. The intracellular fluorescence signal slowly decreased along with the time, and a substantial amount of fluorescent signal was detected even at 24 h (Figure 5E). The fluorescence decrease of the CpG–NMOFs is due to their gradual clearance. Quantitative analysis with flow cytometry indicated that the intracellular FAM fluorescence intensities were ≈16.1-fold and 5.4-fold higher than that for free CpG ODNs at 5 and 24 h, respectively (Figure 5F). Such enhanced intracellular retention of CpG–NMOFs could be attributed to the resistance to nuclease degradation.[40]

To assess the immunostimulatory activity induced by CpG–NMOFs, we measured the levels of secreted cytokines (tumor necrosis factor alpha (TNF-α) and interleukin 6 (IL-6)) generated

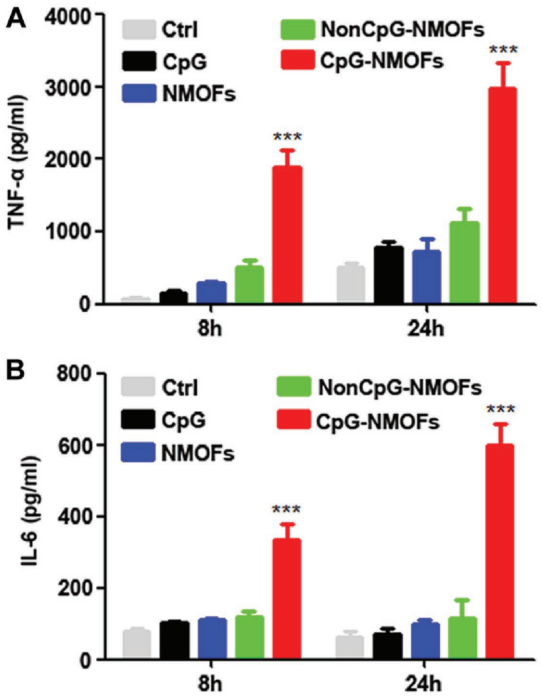

Figure 6. A,B) Cytokine secretion by RAW264.7 cells upon treatment with indicated materials at a DNA concentration of 0.5×10^{-6} M. The generation of A) TNF-α and B) IL-6 were measured immediately or at 24 h after the initial 8 h incubation. Data are represented as means ± SD, $n = 4$, asterisks indicate $P < 0.001$.

from CpG–NMOFs treated RAW264.7 macrophages by enzyme-linked immunosorbent assay (**Figure 6**A,B). After 8 h treatment, CpG–NMOFs carrying the same amount of CpG significantly increased the secreted levels of TNF-α and IL-6 by 12.1-fold and 3.3-fold, respectively, compared with free CpG ODNs. In addition, control studies using a non-CpG sequence-modified NMOFs (NonCpG–NMOFs) exerted much less effect on cytokine secretion, indicating that the observed immunostimulatory activities were indeed induced by the CpG motif on the CpG–NMOFs. We further evaluated the immunostimulatory sustainability by removing noninternalized CpG–NMOFs after 8 h incubation and then measuring the cytokine expression at 24 h. The results showed that the TNF-α/IL-6 expression elicited by CpG–NMOFs was much higher than that induced by the controls, suggesting the sustained and enhanced immunostimulatory activity of CpG–NMOFs, which could be attributed to their high cellular uptake efficiency and slow cellular clearance ability.

The excellent immunostimulatory activity of CpG–NMOFs in vitro motivated us to further investigate their in vivo behaviors. Different samples were administrated at a dose of about 0.5 mg kg^{-1} of CpG into mice by tail-vein injection. Immunostimulatory activity was evaluated 24 h postinjection by measuring the secreted levels of cytokines in serum. As shown in **Figure 7**A,B, mice receiving CpG ODNs showed minimum response and were similar to the unimmunized control group. In contrast, the amount of serum IL-12 and IL-6 at 24 h after administration of CpG–NMOFs was much higher than that of the CpG ODNs, demonstrating that the immunostimulatory activity of the CpG ODNs can be effectively enhanced. In addition, NMOFs

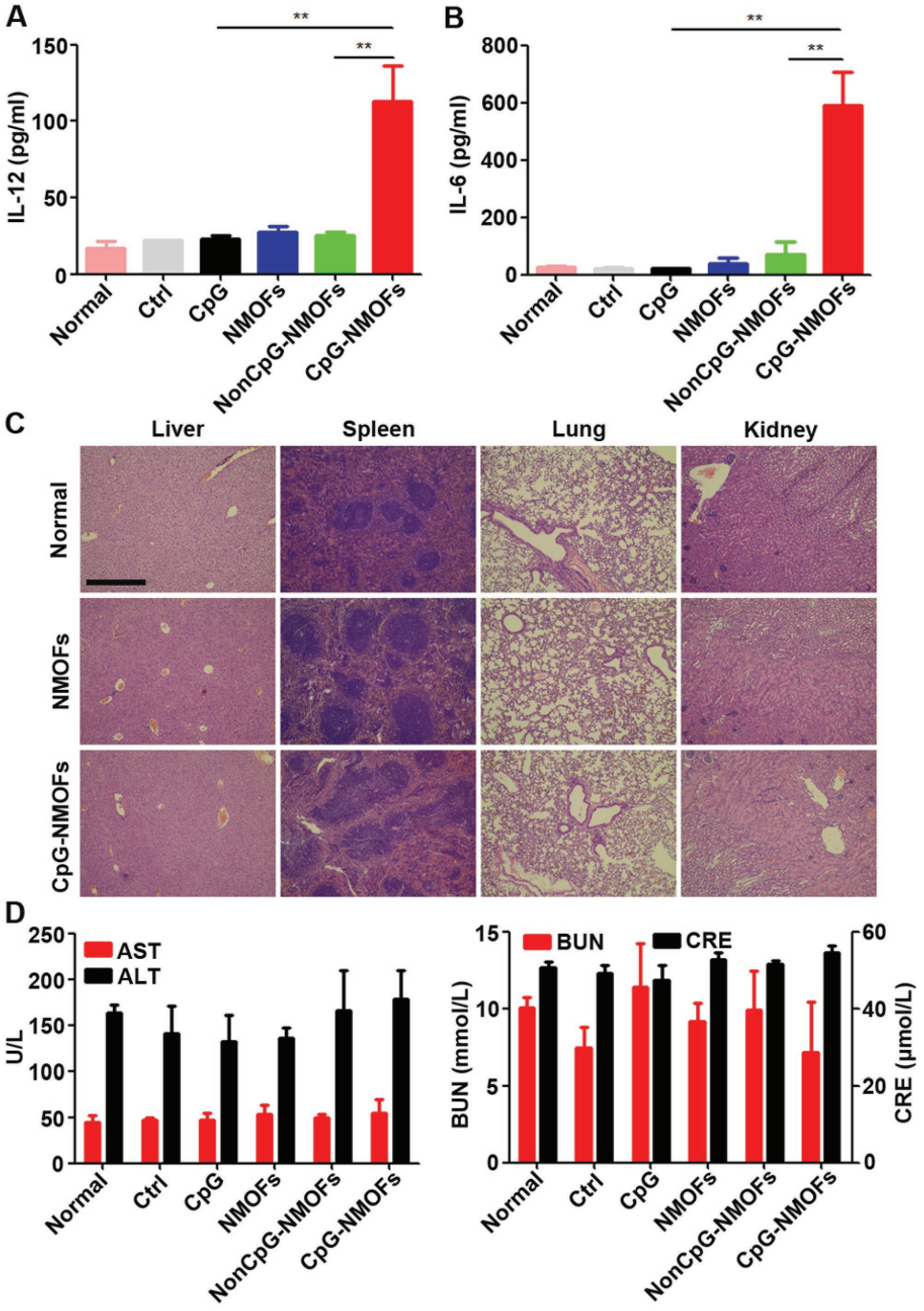

Figure 7. A) Serum IL-12 and B) serum IL-6 levels of mice at 24 h after tail vein injection of indicated materials. Data are represented as means ± SD, $n = 4$, asterisks indicate $P < 0.01$. C) Representative H&E-stained tissue sections from mice to monitor the histological changes in liver, spleen, lung, and kidney at 24 h after tail vein injection of indicated materials. Scale bars = 100 μm. D) Analysis of biochemical parameters in serum after different treatments. Data are represented as means ± SD, $n = 4$.

conjugated with a non-CpG sequence showed no significant increase in cytokine secretion compared to levels in untreated mice. This result corresponds well with our in vitro experiment, confirming that the formation of CpG–NMOF conjugates is a critical factor for the enhanced immunostimulation effects.

Next, we performed a series of in vivo biocompatibility tests to investigate the safety of CpG–NMOFs. Healthy mice with a single intravenous injection of CpG–NMOFs at a dosage of a 15 mg kg^{-1} were euthanized and the major organs were harvested for hematoxylin and eosin (H&E)-stained sections. No noticeable signs of tissue damage or inflammatory lesions to various organs was observed from that of animals in the treatment groups compared to the unimmunized control group (Figure 7C). We further examined the biochemical parameters

including alanine transferase, aspertate aminotransferase, blood urea nitrogen, and creatinine. There is also no significant variation of these parameters between the treatment groups and the control group (Figure 7D). These results provide a preliminary proof that DNA–NMOFs were benign in vivo and showed more promising for further immunotherapy.

The porphyrin-based NMOFs used here have been reported as efficient photosensitizers (PSs) for photodynamic therapy (PDT) of cancer because the porous crystalline structure of NMOFs could facilitate high PS loadings and intersystem crossing to enhance $^1O_2$ production.[15,16] Local PDT has also been shown to induce antitumor immunity due to the acute inflammatory response and induction of various danger signals,[42,43] which has motivated a new strategy by combining immunotherapeutic adjuvants with PDT to enhance cancer immunotherapy.[44,45] Since CpG has been proven to be a valuable immunoadjuvant to combine with PDT,[46] the CpG-functionalized porphyrinic MOFs demonstrated in this work may provide a promising platform for PDT-based synergetic immunotherapy of tumors.

In conclusion, we have developed a very simple strategy to impart biorecognition functionality to NMOFs through functional DNA-mediated surface engineering of MOFs. We have shown that the DNA aptamer-attached NMOFs can be used for targeted imaging of cancer cells. The DNA–NMOFs can be readily taken up by cells without the need of transfection agents, and their use as nanocarriers for therapeutic DNA delivery are also demonstrated. The multivalent CpG–NMOF nanoconjugates efficiently stimulate the antigen-presenting macrophage cells and lead to enhanced immunostimulatory activity in vitro and in vivo. Therefore, we believe that immobilization via coordination chemistry offers a new strategy for producing MOFs with a polyvalent DNA surface, which not only allows insights into the biointerfaces, but also may find wide applications in biosensor, bioimaging, and nanomedicine.

Supporting Information

Supporting Information is available from the Wiley Online Library or from the author.

Acknowledgements

W.N., Z.D., and Y.Y. contributed equally to this work. This work was financially supported by the NSFC (No. 21771044) and the Young Thousand Talented Program.

Conflict of Interest

The authors declare no conflict of interest.

Keywords

biorecognition, DNA, metal–organic frameworks, surface engineering

Received: November 1, 2017
Revised: December 20, 2017
Published online:

[1] H. Furukawa, K. E. Cordova, M. O'Keeffe, O. M. Yaghi, *Science* **2013**, *341*, 1230444.
[2] H.-C. Zhou, J. R. Long, O. M. Yaghi, *Chem. Rev.* **2012**, *112*, 673.
[3] H.-C. Zhou, S. Kitagawa, *Chem. Soc. Rev.* **2014**, *43*, 5415.
[4] P. Horcajada, T. Chalati, C. Serre, B. Gillet, C. Sebrie, T. Baati, J. F. Eubank, D. Heurtaux, P. Clayette, C. Kreuz, J.-S. Chang, Y. K. Hwang, V. Marsaud, P.-N. Bories, L. Cynober, S. Gil, G. Férey, P. Couvreur, R. Gref, *Nat. Mater.* **2010**, *9*, 172.
[5] C. He, D. Liu, W. Lin, *Chem. Rev.* **2015**, *115*, 11079.
[6] P. Horcajada, R. Gref, T. Baati, P. K. Allan, G. Maurin, P. Couvreur, G. Férey, R. E. Morris, C. Serre, *Chem. Rev.* **2012**, *112*, 1232.
[7] F.-K. Shieh, S.-C. Wang, C.-I. Yen, C.-C. Wu, S. Dutta, L.-Y. Chou, J. V. Morabito, P. Hu, M.-H. Hsu, K. C.-W. Wu, C.-K. Tsung, *J. Am. Chem. Soc.* **2015**, *137*, 4276.
[8] J. Zhuang, C.-H. Kuo, L.-Y. Chou, D.-Y. Liu, E. Weerapana, C.-K. Tsung, *ACS Nano* **2014**, *8*, 2812.
[9] H. Zheng, Y. Zhang, L. Liu, W. Wan, P. Guo, A. M. Nyström, X. Zou, *J. Am. Chem. Soc.* **2016**, *138*, 962.
[10] K. Liang, R. Ricco, C. M. Doherty, M. J. Styles, S. Bell, N. Kirby, S. Mudie, D. Haylock, A. J. Hill, C. J. Doonan, P. Falcaro, *Nat. Commun.* **2015**, *6*, 7240.
[11] V. Lykourinou, Y. Chen, X.-S. Wang, L. Meng, T. Hoang, L.-J. Ming, R. L. Musselman, S. Ma, *J. Am. Chem. Soc.* **2011**, *133*, 10382.
[12] M. H. Teplensky, M. Fantham, P. Li, T. C. Wang, J. P. Mehta, L. J. Young, P. Z. Moghadam, J. T. Hupp, O. K. Farha, C. F. Kaminski, D. Fairen-Jimenez, *J. Am. Chem. Soc.* **2017**, *139*, 7522.
[13] A. J. Howarth, Y. Liu, P. Li, Z. Li, T. C. Wang, J. T. Hupp, O. K. Farha, *Nat. Rev. Mater.* **2016**, *1*, 15018.
[14] Y. Bai, Y. Dou, L.-H. Xie, W. Rutledge, J.-R. Li, H.-C. Zhou, *Chem. Soc. Rev.* **2016**, *45*, 2327.
[15] J. Park, Q. Jiang, D. Feng, L. Mao, H.-C. Zhou, *J. Am. Chem. Soc.* **2016**, *138*, 3518.
[16] K. Lu, C. He, W. Lin, *J. Am. Chem. Soc.* **2014**, *136*, 16712.
[17] J. Jiang, Y. Zhao, O. M. Yaghi, *J. Am. Chem. Soc.* **2016**, *138*, 3255.
[18] S. M. Cohen, *J. Am. Chem. Soc.* **2017**, *139*, 2855.
[19] R. Röder, T. Preiß, P. Hirschle, B. Steinborn, A. Zimpel, M. Höhn, J. O. Rädler, T. Bein, E. Wagner, S. Wuttke, U. Lächelt, *J. Am. Chem. Soc.* **2017**, *139*, 2359.
[20] C. Doonan, R. Riccò, K. Liang, D. Bradshaw, P. Falcaro, *Acc. Chem. Res.* **2017**, *50*, 1423.
[21] P. Deria, J. E. Mondloch, E. Tylianakis, P. Ghosh, W. Bury, R. Q. Snurr, J. T. Hupp, O. K. Farha, *J. Am. Chem. Soc.* **2013**, *135*, 16801.
[22] P. Deria, W. Bury, I. Hod, C. W. Kung, O. Karagiaridi, J. T. Hupp, O. K. Farha, *Inorg. Chem.* **2015**, *54*, 2185.
[23] J. E. Mondloch, W. Bury, D. Fairen-Jimenez, S. Kwon, E. J. DeMarco, M. H. Weston, A. A. Sarjeant, S. T. Nguyen, P. C. Stair, R. Q. Snurr, O. K. Farha, J. T. Hupp, *J. Am. Chem. Soc.* **2013**, *135*, 10294.
[24] W. Bury, D. Fairen-Jimenez, M. B. Lalonde, R. Q. Snurr, O. K. Farha, J. T. Hupp, *Chem. Mater.* **2013**, *25*, 739.
[25] O. Karagiaridi, W. Bury, A. A. Sarjeant, C. L. Stern, O. K. Farha, J. T. Hupp, *Chem. Sci.* **2012**, *3*, 3256.
[26] O. Karagiaridi, M. B. Lalonde, W. Bury, A. A. Sarjeant, O. K. Farha, J. T. Hupp, *J. Am. Chem. Soc.* **2012**, *134*, 18790.
[27] S. Takaishi, E. J. DeMarco, M. J. Pellin, O. K. Farha, J. T. Hupp, *Chem. Sci.* **2013**, *4*, 1509.
[28] T. Li, M. T. Kozlowski, E. A. Doud, M. N. Blakely, N. L. Rosi, *J. Am. Chem. Soc.* **2013**, *135*, 11688.
[29] M. Kim, J. F. Cahill, Y. X. Su, K. A. Prather, S. M. Cohen, *Chem. Sci.* **2012**, *3*, 126.
[30] P. Deria, W. Bury, J. T. Hupp, O. K. Farha, *Chem. Commun.* **2014**, *50*, 1965.
[31] C. He, K. Lu, D. Liu, W. Lin, *J. Am. Chem. Soc.* **2014**, *136*, 5181.

[32] S. Wang, C. M. McGuirk, M. B. Ross, S. Wang, P. Chen, H. Xing, Y. Liu, C. A. Mirkin, *J. Am. Chem. Soc.* **2017**, *139*, 9827.
[33] L. He, M. Brasino, C. Mao, S. Cho, W. Park, A. P. Goodwin, J. N. Cha, *Small* **2017**, *13*, 1700504.
[34] Z. Wang, Y. Fu, Z. Kang, X. Liu, N. Chen, Q. Wang, Y. Tu, L. Wang, S. Song, D. Ling, H. Song, X. Kong, C. Fan, *J. Am. Chem. Soc.* **2017**, *139*, 15784.
[35] J. H. Lee, M. V. Yigit, D. Mazumdar, Y. Lu, *Adv. Drug Delivery Rev.* **2010**, *62*, 592.
[36] S. Soundararajan, W. Chen, E. K. Spicer, N. Courtenay-Luck, D. J. Fernandes, *Cancer Res.* **2008**, *68*, 2358.
[37] A. B. Chinen, C. M. Guan, C. A. Mirkin, *Angew. Chem., Int. Ed.* **2015**, *54*, 527.
[38] D. M. Klinman, *Nat. Rev. Immunol.* **2004**, *4*, 249.
[39] J. Vollmer, A. M. Krieg, *Adv. Drug Delivery Rev.* **2009**, *61*, 195.
[40] J. I. Cutler, E. Auyeung, C. A. Mirkin, *J. Am. Chem. Soc.* **2012**, *134*, 1376.
[41] M. Wei, N. Chen, J. Li, M. Yin, L. Liang, Y. He, H. Song, C. Fan, Q. Huang, *Angew. Chem., Int. Ed.* **2012**, *51*, 1202.
[42] P. C. Kousis, B. W. Henderson, P. G. Maier, S. O. Gollnick, *Cancer Res.* **2007**, *67*, 10501.
[43] A. P. Castano, P. Mroz, M. R. Hamblin, *Nat. Rev. Cancer* **2006**, *6*, 535.
[44] X. Duan, C. Chan, N. Guo, W. Han, R. R. Weichselbaum, W. Lin, *J. Am. Chem. Soc.* **2016**, *138*, 16686.
[45] K. Lu, C. He, N. Guo, C. Chan, K. Ni, R. R. Weichselbaum, W. Lin, *J. Am. Chem. Soc.* **2016**, *138*, 12502.
[46] Y. Xia, G. K. Gupta, A. P. Castano, P. Mroz, P. Avci, M. R. Hamblin, *J. Biophotonics* **2014**, *7*, 897.